Desalination and Water Treatment
www.deswater.com
doi: 10.5004/dwt.2019.22848

144 (2019) 1–8
March

Simulation of multiphysics field and analysis of electrosorption characteristics in capacitive desalination

Shou-Guang Yao*, Ji-Wen Wu

School of Energy and Power Engineering, Jiangsu University of Science and Technology, Zhenjiang, Jiangsu 212003, China, Tel. +86 15-051-110-000; email: zjyaosg@126.com (S.-G. Yao), Tel. +86 18-810-322-826; email: jsdywjw@163.com (J.-W. Wu)

Received 6 December 2017; Accepted 21 July 2018

ABSTRACT

Simulation of multiphysics field was carried out for seawater desalination using capacitive deionization (CDI). For the multiphysics field of a CDI unit capacitance electrode, a mathematical model was constructed using transient coupling analysis. The flow field, concentration field, and potential distribution within the CDI electrode were determined, and the pattern of adsorption on the electrode plate and mass transfer process in solution in the CDI unit was studied. In addition, the effects of different voltages, plate spacings, inlet flow rates, inlet concentrations, and porous materials on the adsorption of the CDI unit were investigated. The higher the voltage between the plates, the smaller the plate spacing. A lower inlet flow rate improved the performance of the CDI desalination unit. With all other parameters fixed, the adsorption performance and desalination efficiency of the CDI desalination unit mainly depended on the conductivity and pore structure of the porous electrode materials. When the porous electrode pore parameters and conductivity were fixed, the adsorption and desalination efficiency of the CDI desalination unit remained unchanged. Excellent adsorption and optimal desalination could be achieved using highly conductive porous electrode materials, which possessed a medium hole structure and the maximum surface area.

Keywords: Capacitive deionization; Porous electrode; Modeling

1. Introduction

Capacitive deionization (CDI), a new technology for seawater desalination, uses an electric double layer (EDL) formed at the interface between the electrode and the solution for desalination, in which ions are forced to move to the electrode side, resulting in an effluent product stream with a reduced ion concentration (Fig. 1) [1]. The charged species can be released back into the flow solution when the potential difference is reversed or removed. This technology requires a simple device and has low energy consumption and a low operation cost; it also produces no secondary pollutants. Therefore, it can be used for desalination [2]. Oda and Nakagawa [3] found that the electrosorption ("adsorption" for short) capacity of an activated carbon (AC) electrode surface is determined by the pore size and specific surface area of AC, and the amount of ions removed corresponds to the surface area. Kötz et al. [4] proved that double layer capacitors with high-surface-area ACs have low capacitance limits, and their differential capacitance functions exhibit extreme points. The first CDI plant was designed by Caudle et al. [5], using series electrodes made of AC materials. Although they were able to remove the ions from solution, it was not significant. At that time, the carbon material used to be scarce and also suffer from poor stability, among other issues, which limited the development of the CDI desalination technology. In recent years, new materials have been developed, which have helped rapid development of the CDI desalination technology [9–11]. Xin et al. [12] found that ions with smaller hydrated

* Corresponding author.

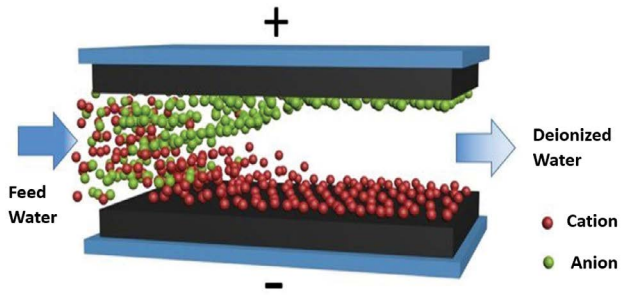

Fig. 1. Schematic view of one CDI cell.

radius exhibited higher removal efficiency with lower energy consumption, and the difference of hydrated radius can be further enhanced when increasing the working voltage. Lang et al. [13] fabricated flexible and free-standing electrode by depositing SR-PE2 onto a nonwoven carbon nanotube textile (CNT-T), and assembled into symmetrical, flexible supercapacitors where the addition of polymer resulted in a boost in volumetric capacitance by 400% compared with the bare CNT-T electrode. Wu et al. [14] prepared an electrode material by chemical oxidation of polypyrrole/CNTs using the CDI desalination technology. The chemically modified polypyrrole/CNTs showed higher specific capacitance than polypyrrole and their good mechanical properties and electrical conductivity helped achieve an electrosorption capacity of 21.55 mg/g for Na^+ during the charging period. Khan et al. [15] prepared 3D intercalated graphene sheet–sphere nanocomposite architectures as high-performance CDI electrodes by using graphene oxide and [Ni_2(EDTA)] as precursors. By using 3D mesoporous graphene sheet–sphere nanocomposite architectures as an electrode, an ultrahigh electrosorptive capacity of 22.09 mg/g is achieved in a 500 mg/L NaCl solution at 1.2 V. Hu [24] made use of activated carbon fiber (ACF) electrode to study the desalination efficiency of CDI unit, which achieved only 8.3% Cl^- removal efficiency. The removal efficiency of other ions using ACF electrode unit electric adsorption was analyzed, as well as a preliminary explore for enhancing the desalination efficiency for ACF electrode electric adsorption. However, current studies on CDI desalination are still at the experimental stage [16–19].

In a recent publication, Suss [32] extended the existing models by accounting for ion volume exclusion interactions to demonstrate selective ion removal based on ion size, in the area of EDLs modeling. Tang et al. [33] studied the removal of sulfate in MCDI and observed more sulfate removal in a mixture of sulfate and chloride with equal molar concentrations. As diffusion of the ions through the IEMs occurs prior to ion adsorption inside the micropores, these are crucial in controlling the diffusion. Moreover, multiphysics numerical analysis for CDI electrode adsorption/desorption processes and the analysis of the mechanism involved [20–22] are not sufficient. Thus, the impact factors of CDI desalination and the mechanism of action are still not clear.

In this study, we investigate mass transfer in solution in a porous cell electrode in a seawater desalination unit, charge transfer between the plates, and various interactions involve in the porous adsorption process on the plate. We utilize the coupling of the different principles of mass, momentum, and charge conservation; the porous Darcy flow equation; and the kinetic equation to construct a transient analysis model employing multiphysics coupling in the desalination process in a CDI unit. The effects of different working voltages, plate spacings, inlet flow rates, inlet concentrations, and porous electrode on the desalting performance of the CDI electrode are investigated by numerical simulation.

2. Physical model and parameters

Fig. 2(a) shows a schematic diagram of the three-dimensional structure of a CDI desalination unit (100 mm wide and 300 mm long). In Fig. 2(b), the red cuboid represents the negative electrode, the green cuboid represents the positive electrode, and the middle is the flow channel. The thickness of the monolithic porous electrode is 0.4 mm. The length of the X direction is defined as the thickness of the CDI unit, the length of the Y direction is the width of the CDI unit, and the length of the Z direction is the length of the CDI unit.

Since the positive and negative electrodes of the CDI desalination unit are porous materials, the flow channel and the positive and negative plates are filled with the electrolyte solution. We divided the CDI unit into three parts: the positive electrode, the negative electrode, and the flow channel. The positive and negative plates comprised biphasic solid–liquid components: the solid phase was a porous material and the liquid phase was Na or Cl ions in solution for mass transfer in the porous plate. The fluid flow,

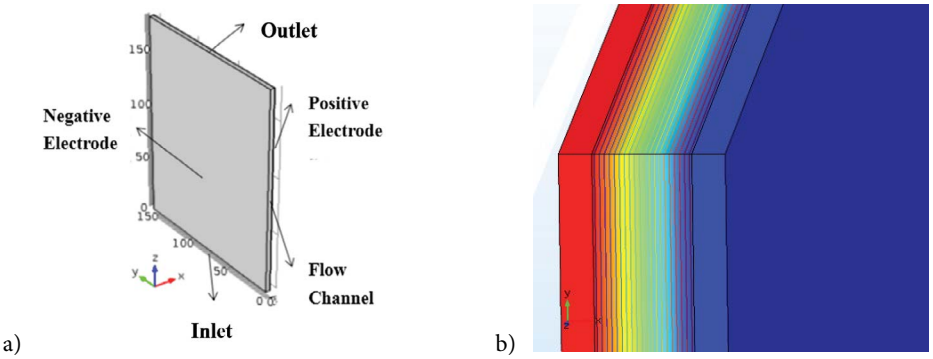

Fig. 2. (a) Capacitive deionization unit used in this study. (b) A corner of the capacitive deionization unit 3D structure.

mass transfer, and charge transfer occurred within the flow channel.

The main parameters used in the model analysis are listed in Table 1.

3. Mathematical model and boundary conditions

3.1. Model assumptions

We made the following assumptions:

- Effects from gravity were neglected.
- Side reactions such as hydrogen and oxygen evolutions were not considered.
- The fluid flow was treated as an incompressible flow.
- Physical properties of the electrode and solution were isotropic and homogeneous.
- An isothermal condition was assumed for all domains.

3.2. Model validation

In order to verify the correctness of the model for multiphysics coupling simulation analysis of the capacitance method used in the seawater desalination unit, we determined the desalination curves at different voltages changes with time for the inlet concentration of C^{ref} = 500 mol/m^3, inlet velocity of 0.1 m/s, and plate spacing δ = 0.5 mm (as shown in Fig. 3), using Langmuir isothermal adsorption equation for linear regression of the first-order adsorption rate equation.

The adsorption equilibrium concentration C_e and the adsorption amount q were substituted into the linear form (Eq. (1)) of the Langmuir adsorption isothermal equation (Eq. (2)), and the q_m and b values were obtained at different voltages.

$$q = \frac{q_m b C_e}{1 + bC_e} \tag{1}$$

$$\frac{1}{q} = \frac{1}{q_m b C_e} + \frac{1}{q_m} \tag{2}$$

Here q is the adsorption capacity (mg/g); q_m is adsorption saturation (mg/g); b is Langmuir adsorption constant (L/mg); and the quantity of carbon electrode used in simulation was 13.56 g.

The results are shown in Table 2. The average correlation coefficient R^2 = 0.90, and the adsorption rate accorded with that obtained using Langmuir first-order kinetics [24]. In summary, the multiphysics coupling model proposed in this paper is suitable for the numerical simulation of CDI desalination unit.

Table 1
Main parameters of model simulation

Parameter	Value
Solution viscosity (Pa s)	0.003139
Na^+ diffusion coefficient (m^2/s)	2.5×10^{-9}
Cl^- diffusion coefficient (m^2/s)	2×10^{-10}
Ambient temperature (K)	295.13
Conductivity of solution (S/m)	1

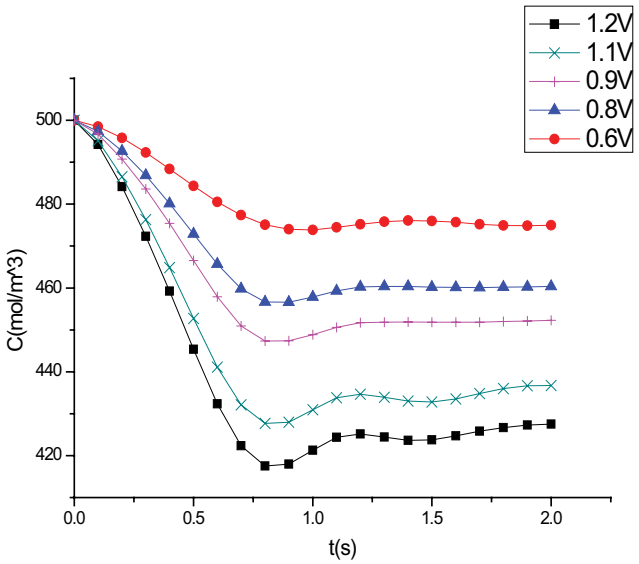

Fig. 3. Sodium ion concentration curves at the outlet under different voltages.

Table 2
Parameters for the estimation of Langmuir adsorption isothermal equation

Voltage	q_m	$b \times 10^5$	R^2
0.6	9.4	19.3	0.863
0.8	23.7	7.9	0.844
0.9	35.1	5.4	0.897
1.1	46.2	4.3	0.931
1.2	51.0	4.0	0.945

3.3. Basic control equation

The physical model, established by a desalination unit and composed of a flow channel, a positive electrode, a negative electrode, and an electrolyte, was used to describe the physical processes involved in the flow of the solution, adsorption of the solution with the electrode, and transfer of the solute of the solution to the CDI desalination unit, by coupling the principles of mass, momentum, and charge conservation, and by using the porous Darcy flow equation and the adsorption kinetic equation.

Continuity equation:

$$\nabla\left(\vec{u}\right) = 0 \tag{3}$$

Momentum conservation equation:

$$\nabla \cdot \left(\rho \vec{u}\vec{u}\right) = -\nabla p + \nabla \cdot \left(\mu \nabla \vec{u}\right) \tag{4}$$

Since the solution is assumed to be a dilute solution, the viscosity coefficient μ is constant.

The process of liquid phase mass transfer through the flow channel involves three stages: convection, diffusion, and electric field migration. The efficiency of the convective mass transfer is the highest. Fick's law can be used to describe the diffusive transport. The Nernst–Planck equation is used to describe electric field migration in the solution. The last term in parentheses represents convection.

Liquid phase [23]:

$$\nabla\cdot\left(-D_i\nabla C_i - Z_i\frac{D_i}{RT}\right)FC_i\nabla\varphi_l + \vec{u}C_i = R_i \tag{5}$$

The convection is not considered in the mass transfer process of the porous electrodes, and therefore, the mass transfer equation can be expressed as follows:

Solid phase:

$$\nabla\cdot\left(-D_i^{eff}\nabla C_i - Z_i\frac{D_i^{eff}}{RT}\right)FC_i\nabla\varphi_s = R_i \tag{6}$$

where p is the fluid pressure, $\vec{u}$ is the velocity vector, ρ is the fluid density, μ is the dynamic viscosity, D_i denotes the diffusion coefficient of species i; C_i denotes the concentration of species i; $i\in\{Na^+, Cl^-\}$; Z_i denotes the charge of species i; ϕ_s and ϕ_l denote the potential of the solid and the liquid phase, respectively; and R_i denotes the component source term of species i.

Eqs. (5) and (6) can be expressed as ion transport flux as follows [23]:

$$\vec{N}_{i1} = -D_i\nabla C_i - Z_i\frac{D_i}{RT}FC_i\nabla\varphi_l + \vec{u}C_i \tag{7}$$

$$\vec{N}_{i2} = -D_i^{\text{eff}}\nabla C_i - Z_i\frac{D_i^{\text{eff}}}{RT}FC_i\nabla\varphi_l \tag{8}$$

where $\vec{N}_i$ is flux, which denotes the flow rate of the diffused substance per unit time through the unit cross-sectional area perpendicular to the diffusion direction; D_i^{eff} is the effective diffusion coefficient in the porous electrode, expressed by the Bruggemann correction equation as follows [20]:

$$D_i^{\text{eff}} = \varepsilon^{3/2}D_i \tag{9}$$

The value of $\vec{u}$ is calculated by the Darcy formula as follows [22]:

$$\vec{u} = -\frac{d_f^2}{K\mu}\times\frac{\varepsilon^3}{\left(1-\varepsilon\right)^2}\nabla p \tag{10}$$

where K is the permeability of the porous media, which is often described by the Carman–Kozeny equation as follows [29]:

$$K = \frac{d_f^2\varepsilon^3}{16k_{\text{CK}}\left(1-\varepsilon\right)^2} \tag{11}$$

The electromigration equation can be written in the following form:

$$D = \varepsilon_0\left(1+\chi_e\right)\quad E = \varepsilon_0\varepsilon_r E \tag{12}$$

where χ_e is the electric susceptibility and D is the electric displacement.

3.4. Boundary conditions

At the entrance of the CDI unit, both the speed and concentration of the solution were uniform.

The fluid–solid interface was a no-slip boundary:

$$\vec{u} = 0 \tag{13}$$

At the exit, the boundary condition of the solution was set to the pressure of the outlet boundary, and the diffusion flux of each substance was set to zero, and then, the boundary condition was given by the following:

$$p_{-\text{out}} = 0 \text{ and } -n\cdot D_i\nabla c_i = 0,\ \text{z} = 300\,\text{mm} \tag{14}$$

The electrode potential boundary was set as follows:

$$\begin{cases}\varphi\left(x\right) = \varphi_0, x = 0;\\ \varphi\left(\infty\right) = 0, x = \infty\end{cases} \tag{15}$$

The initial conditions for the concentration of each component of the solution in the domain were given by the following:

$$C_i = C^{\text{ref}} \tag{16}$$

where $p_{-\text{out}}$ is the pressure of the outlet and C^{ref} denotes the concentration of the initial substance.

4. Analysis and comparison of simulation results

In Sections 4.1–4.4, we first describe the simulation of the porous electrode material using the following parameters: electrode porosity epsilon, ε = 40%; permeability (which is the reciprocal of the pore density), κ = 0.9 × 10^{-10}; and conductivity, K = 450 S/m for the AC material. Using the control variable method, we changed a single parameter (working voltage, plate spacing, inlet velocity, and inlet concentration) that affected the desalination performance of the CDI unit. Then, in Section 4.5, we discuss the changes in the porous electrode material that we simulated to determine the impact of porous electrode materials with different parameters (shown in Table 3) on the desalination performance of the CDI unit.

4.1. Effect of voltage on adsorption desalination

Since electrolysis of water might occur at voltages higher than 1.2 V [30,31], the simulated voltages were 0.6, 0.8, 0.9, 1.1, and 1.2 V. Fig. 3 shows how the average Na^+ concentration of the desalting unit at different voltages changes with time

for the inlet concentration of C^{ref} = 500 mol/m^3, inlet velocity of 0.1 m/s, and plate spacing δ = 0.5 mm. It is seen that in the voltage range of 0.6–1.2 V, the adsorption rate accelerated with increase in the voltage. The average Na^+ concentration at the outlet decreased gradually, that is, the adsorption capacity of NaCl enhanced. At the maximum voltage of 1.2 V, the adsorption efficiency of NaCl solution was the highest. This implied that the higher the applied voltage of the electrode, the better was the desorption performance of the CDI desalting unit, without occurrence of water electrolysis. This is because both the charge in the interchannel flow and the thickness of the EDL increased with increasing voltage [24], which enhanced the ion adsorption capacity.

4.2. Effect of plate spacing on adsorption desalination

Plate spacing values used in the simulation were 0.5, 0.6, 0.8, 1, and 1.2 mm. Fig. 4 shows how, at the inlet concentration C^{ref} = 500 mol/m^3, inlet velocity of 0.1 m/s, and interplate voltage of 1.2 V, the average Na^+ concentration of the desalting unit under different plate spacings changed with time. The figure shows that with decreasing plate spacing, the desalination effect gradually increased. The adsorption efficiency of the NaCl solution was the highest when the plate spacing was δ = 0.5 mm. This is because, for a constant width of the plate, changing the plate spacing changed the ion lateral diffusion distance. As the plate spacing became smaller, the ion transport resistance reduced, making the ions more favorable for adsorption by the two porous plates [24]. Therefore, when other conditions remain unchanged, the plate spacing should be minimized in order to improve the CDI desalination performance.

4.3. Effect of inlet velocity on adsorption desalination

The inlet flow rates used for the desalting units were 0.08, 0.09, 0.1, 0.11, and 0.12 m/s. Fig. 5 shows how, at the inlet concentration of C^{ref} = 500 mol/m^3, plate spacing of

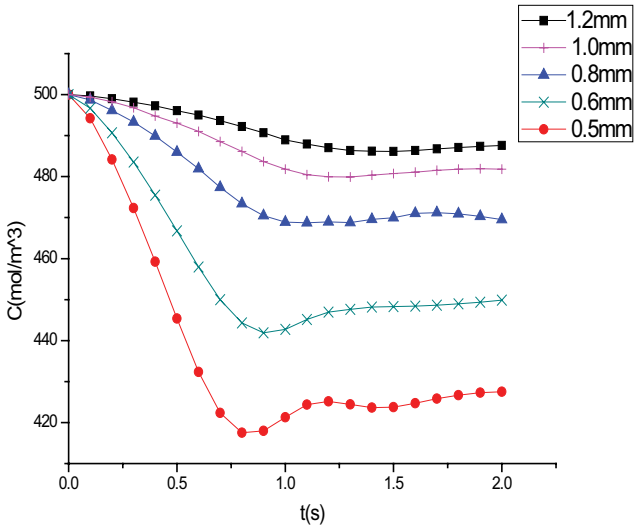

Fig. 4. Sodium ion concentration curves at the outlet for different plate spacings.

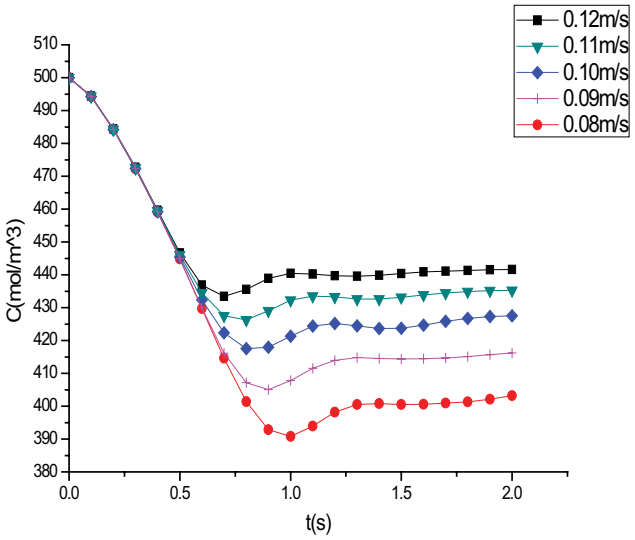

Fig. 5. Sodium ion concentrations at different inlet flow rates.

δ = 0.5 mm, and inter-plate voltage of 1.2 V, the average Na^+ concentration of the desalting unit under different inlet velocities changed with time. When the inlet velocity was 0.08 m/s, the adsorption efficiency of NaCl solution was the highest. With increase in the inlet velocity, the concentration of Na^+ in the outlet increased and the desalination performance decreased. This was mainly due to the increase in the inlet velocity, which shortened the residence time of the solution in the flow channel. The ions were not completely adsorbed, as the solution flowed out of the device. Thus, the adsorption capacity decreased and the concentration at the outlet increased. Thus, to enhance solution purification and desalination, the choice of a smaller inlet velocity is appropriate. However, in practical applications, if the inlet velocity is too slow, the hydraulic retention time will increase significantly, and then, the time required for desalination of seawater is bound to decrease a lot; thus, trade-offs need to be considered.

4.4. Effect of inlet concentration on adsorption desalination

Because the concentration of seawater varies significantly with the season and the region of the sea, the salt concentrations considered herein were 300, 500, and 700 mol/m^3. Fig. 6 shows how the average Na^+ concentration of the desalting unit under different inlet concentrations changed with time when the inlet velocity was 0.08 m/s, plate spacing was δ = 0.5 mm, and interplate voltage was 1.2 V.

In order to facilitate comparison, salt removal efficiency η was introduced.

$$\eta = \frac{C_0 - C}{C_0} \times 100\% \tag{17}$$

where C is the concentration of the outlet solution (mol/m^3); C_0 is the concentration of the inlet solution (mol/m^3); and η is the desalination efficiency.

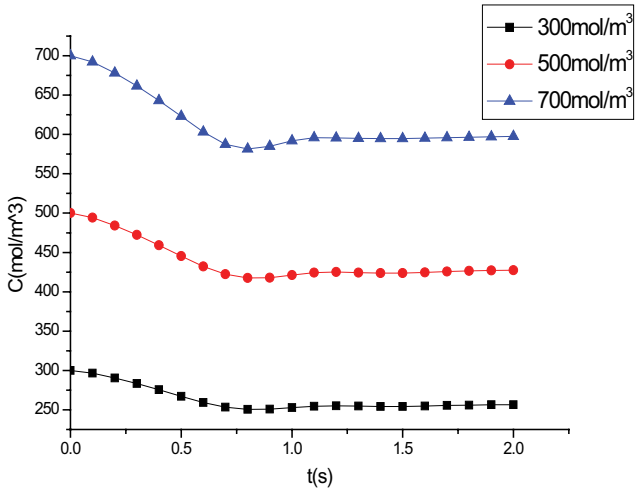

Fig. 6. Concentration of sodium ions at different inlet concentrations.

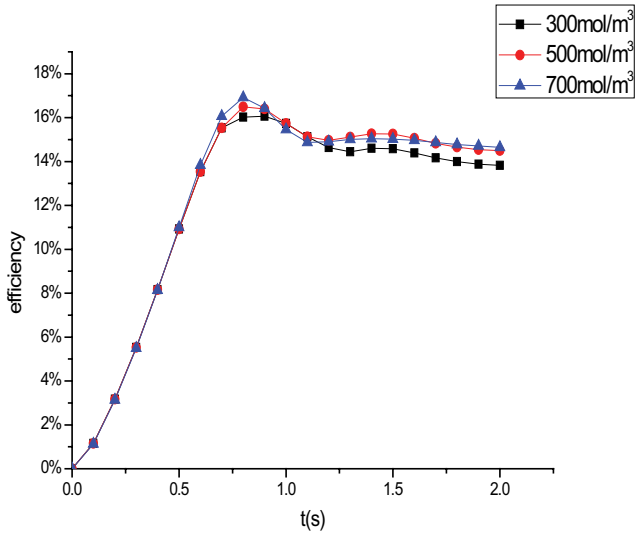

Fig. 7. Salt removal efficiency at different outlet concentrations.

According to the definition of the desalination efficiency, Fig. 6 further shows outlet desalination efficiency curves for different inlet concentrations.

As seen in Fig. 7, the change in the inlet concentration had little effect on the removal efficiency at a given pore material parameter (ε = 40%, $\kappa = 0.9 \times 10^{-10}$, and conductivity = 450 S/m). When all other parameters (design and operating parameters) were fixed, the CDI adsorption desalting performance and efficiency of the desalination unit depended on the porous electrode pore parameters and electric conductivity. When the pore parameters and conductivity of the porous electrodes were fixed, the desalination efficiency of the CDI desalination unit remained unchanged.

4.5. Effect of plate material on adsorption desalination

According to the analysis discussed in Section 3.4, the porosity of the porous electrode plate material and its conductive ability are very important in determining the CDI desalting efficiency, mainly due to the large differences between the different porosities of the macroporous electrode materials ε, permeability κ (which is the reciprocal of the pore density), and electrical conductivity K [25–27]. According to the currently available material parameters, five typical porous electrode plates were selected for simulation, and the specific material parameters are given in Table 3.

Fig. 8 shows the average Na^+ concentration of the desalting unit for different materials when the inlet concentration was C^{ref} = 500 mol/m^3, plate spacing was δ = 0.5 mm, and interplate voltage was 1.2 V. It can be seen that after activation treatment of the graphene electrode, it provided the best adsorption performance and best desalting efficiency, owing to the stable two-dimensional hexagonal planar structure, the dimension of the pore structure, and larger pores, which led to higher pore density and a large specific surface area. At the same time, the graphene electrode itself has excellent electrical conductivity, and further enhancement in the conductivity showed that graphene, as a porous electrode plate material, has advantages that other materials cannot match. For example, woodiness AC materials have a large number of micropores, and the pore size is mostly less than 10 nm, and the pore density is much higher than that of graphene. Although the pore size can lead to a larger specific electrode surface area, the "overlap effect" [2] easily occurred in the channel, significantly decreasing the utilization ratio of the surface area in the porous material, which deteriorated the desalination performance. Moreover, the conductivity of the electrode materials not subjected to activation showed great changes. It was seen that after activation modification, both the electrode conductivity and the amount of electric migration increased, which was more conducive to desalination. This suggests that the adsorption performance and desalination efficiency of the CDI desalination unit mainly depended on the conductivity and pore structure of the porous electrode materials. Excellent adsorption performance and optimal desalination efficiency could be achieved for a high

Table 3
Simulation electrode material parameters

Number	Plate material	Porosity ε (%)	Permeability κ	Conductivity K (S/m)
1	Nonactivated shell AC	31.4	6.27×10^{-8}	12
2	Nonactivated woodiness AC	40	0.9×10^{-10}	12
3	Nonactivated graphene	78.7	2.9×10^{-9}	1,000
4	Activated graphene	78.7	2.9×10^{-9}	4,000
5	Activated woodiness AC	40	0.9×10^{-10}	450

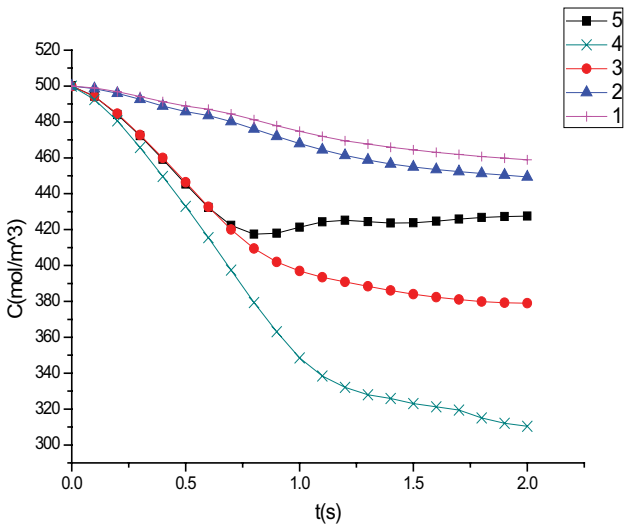

Fig. 8. Sodium ion concentrations for different outlet materials, where number corresponds to the Number column in the Table 3.

conductivity of the porous electrode materials, when the porous materials possessed a medium hole structure and the large specific surface area.

5. Conclusions

Based on a numerical analysis model for a desalination unit, this study carried out a detailed simulation analysis to determine the influence of ion-related parameters on the deionization process of the CDI desalting unit. The following results were obtained:

- Theoretically, the higher the electrode voltage of the CDI desalting unit, the better the desalting effect. Considering that the voltage not only influences the desalting effect, but also affects the energy consumption of the CDI device, when it is higher than the water electrolysis voltage, a side reaction of hydrogen evolution will occur. Thus, the maximum voltage for which water electrolysis would not occur was chosen as the optimum desalination voltage of the CDI desalting unit.
- Reducing the plate spacing was beneficial to the desalination of seawater. However, a small plate spacing resulted in a small channel, leading to a constant flow rate, and hence, the amount of seawater treated per unit time was low. At the same time, difficulty of manufacturing the unit also increased with decrease in plate spacing.
- Theoretically, the lower the inlet velocity of the CDI desalting unit, the better the adsorption desalination effect. However, in actual operation, it is necessary to consider the capacity of desalination of system and units. Therefore, it is necessary to weigh carefully and finally select the appropriate inlet flow rate.
- The adsorption performance and desalting efficiency of the CDI desalination unit were not affected by changes in the inlet concentration for a given design and operation parameters of the CDI desalting unit and porous electrode materials.
- Porous electrode materials are the key factors affecting the CDI desalting effect. Simulation showed that the adsorption performance and desalination efficiency of the CDI desalination unit mainly depended on the conductivity and pore structure of the porous electrode materials. Excellent adsorption performance and optimal desalination efficiency could be achieved with highly conductive porous electrode materials and when the porous materials possessed a medium hole structure and maximum surface area.

Conflicts of interest

There is no conflict of interest to state. The founding sponsors had no role in the design of the study; in the collection, analyses, or interpretation of data; in the writing of the manuscript; and in the decision to publish the results.

Appendix A

Nomenclature

C_i	—	Concentration, mol/m^3
d_f	—	Carbon electrode fiber diameter, m
D_i	—	Diffusion coefficient of species i, m^2/s
F	—	Faraday's constant, C/mol
$\vec{N}_i$	—	Flux, mol/m^2 s
p	—	Fluid pressure, Pa
R	—	Universal gas constant, J/mol K
R_i	—	Component source term of species i, mol/m^3 s
t	—	Time, s
T	—	Temperature, K
$\vec{u}$	—	Velocity vector, m/s
Z_i	—	Charge of species i, dimensionless
D	—	Electric displacement, C/m^2
D_i^{eff}	—	Effective diffusion coefficient in the porous electrode, m^2/s

Greek

ε	—	Porosity of the carbon electrode, dimensionless
ϕ_l	—	Potential of the liquid phase, V
ϕ_s	—	Potential of the solid phase, V
μ	—	Dynamic viscosity, Pa s
χ_e	—	Electric susceptibility, dimensionless

Subscript

in	—	Inlet
out	—	Outlet
X	—	Component in the X direction
Y	—	Component in the Y direction

Superscript

eff	—	Effective value
i	—	Species $i \in \{Na^+, Cl^-\}$

References

[1] J.-X. Muo, Study on the method of capacitive adsorption deionization, Technol. Water Treat., 33 (2007) 20–22.
[2] G.-J. Yin, F.-M. Chen, Progress in capacitive deionization, Technol. Water Treat., 29 (2003) 63–66.

[3] H. Oda, Y. Nakagawa, Removal of ionic substances from dilute solution using activated carbon electrodes, Carbon, 41 (2003) 1037–1047.
[4] O. Barbieri, M. Hahn, A. Herzog, R. Kötz, Capacitance limits of high surface area activated carbons for double layer capacitors, Carbon, 43 (2005) 1303–1310.
[5] D.D. Caudle, J.H. Tucker, J.L. Cooper, B.B. Arnold, A. Papastamataki, Electrochemical demineralization of water with carbon electrodes, Oklahoma Univ. Res. Inst., 4 (1966) 7397–7397.
[6] R. Atlas, Purification of brackish or sea water using electronic water purification, Desal. Water Reuse, 4 (2001) 10–17.
[7] T.J. Welgemoed, C.F. Schutte, Capacitive Deionization Technology™: an alternative desalination solution, Desalination, 183 (2005) 327–340.
[8] H.J. Oh, J.H. Lee, H.J. Ahn, Y. Jeong, Y.J. Kim, Nanoporous activated carbon cloth for capacitive deionization of aqueous solution, Thin Solid Films, 515 (2006) 220–225.
[9] R. Kotz, M. Carlen, Principles and applications of electrochemical capacitors, Electrochim. Acta, 45 (2000) 2483–2498.
[10] Z. Spitalsky, D. Tasis, K. Papagelis, C. Galiotis, Carbon nanotube-polymer composites: chemistry, processing, mechanical and electrical properties, Prog. Polym. Sci., 35 (2010) 357–401.
[11] J.M. Gonzalez-Domínguez, M. González, A. Ansón-Casaos, A.M. Díezpascual, M.A. Gómez, Effect of various aminated single-walled carbon nanotubes on the epoxy cross-linking reactions, J. Phys. Chem., 115 (2011) 7238–7248.
[12] X.-H. Xin, L. Chen, L. Zhu, Y.-P. Qiu, Effects of operating parameters and ion characters on the adsorption capacity and energy consumption in membrane capacitive deionization, Desalination, 108 (2018) 58–64.
[13] A.W. Lang, J.F. Ponder, Jr., A.M. Österholm, N.J. Kennard, R.H. Bulloch, J.R. Reynolds, , Flexible, aqueous-electrolyte supercapacitors based on water-processable dioxythiophene polymer/carbon nanotube textile electrodes, J. Mater. Chem. A., 5 (2017) 23887–23897.
[14] Y.-F. Wu, Y. Wang, Y.-J. Zhao, R.-G. Wang, S.-C. Xu, Preparation and application of DBS-PPy/CNTs composite as cathode material for capacitive deionization process, Technol. Water Treat., 39 (2013) 24–27.
[15] Z.U. Khan, T.-T. Yan, L. Shi, D. Zhang, Improved capacitive deionization by using 3D intercalated graphene sheet–sphere nanocomposite architectures, Environ, Sci. Nano, 5 (2018) 980–991.
[16] H. Duan, T. Yan, G. Chen, J. Zhang, L. Shi, D. Zhang, A facile strategy for the fast construction of porous graphene frameworks and their enhanced electrosorption performance, Chem Commun., 53 (2017) 7465–7468.
[17] S.-H. Li, Y.-Z. Pan, Experimental study on capacitive deionization with activated carbon fiber electrodes, Ind. Water Wastewater, 41 (2014) 27–32.
[18] Z. Wang, T. Yan, L. Shi, D. Zhang, In situ expanding pores of dodecahedron-like carbon frameworks derived from MOFs for enhanced capacitive deionization, ACS Appl. Mater. Interfaces, 9 (2017) 15068−15078.
[19] S.-Q. Shi, Y. Wang, S.-C. Xu, Y.-J. Zhao, Y.-F. Wu, Experimental study on capacitive deionization of graphite ribbon electrode, Technol. Water Treat., 39 (2013) 29–32.
[20] R. Zhao, P.M. Biesheuvel, H. Miedema, H. Bruning, A. van der Wal, Charge efficiency: a functional tool to probe the double-layer structure inside of porous electrodes and application in the modeling of capacitive deionization, J. Phys. Chem. Lett., 1 (2010) 205–210.
[21] Z.-S. Zhou, L. Jiang, L.-W. Wang, R.-Z. Wang, P. Gao, Adsorption/desorption non-equilibrium characteristics of composite $MnCl_2$-NH_3 working pair, J. Shanghai Jiaotong Univ., 60 (2016) 583–587+594.
[22] Z. Zhou, C. Ying, H.-L. Fang, The study on electrochemical polarization of vanadium redox flow battery, Dongfang Electr. Rev., 28 (2014) 1–7.
[23] D.-J. You, H. Zhang, J. Chen, A simple model for the vanadium redox battery, Electrochim. Acta, 54 (2009) 6827–6836.
[24] B.-J. Hu, Application progress of electrode materials in electro adsorption desalination, ChengShi Jianshe LiLun Yan Jiu, 16 (2013) 16–18.
[25] K. Yujin, C. Jaehwan, Improvement of desalination efficiency in capacitive deionization using a carbon electrode coated with an ion-exchange polymer, Water Res., 44 (2010) 990.
[26] L.-L. Liu, A Study of Graphene Used for Constructing Molecular Junctions and Measuring their Conductance, Chongqing University, 2016, pp. 31,32.
[27] Y.-H. Xiang, X.-W. Fu, Q. Tian, Porosity evaluation for porous electrodes using image processing, Chin. J. Power Sources, 40 (2016) 572–574.
[28] K. Huang, H. Tang, D.-Y. Liu, S.-Y. Zhu, Z.-Y. Ren, Review of capacitive deionization technology (second): electrode materials, Environ. Eng., 34 (2016) 89–100+77.
[29] M.M. Tomadakis, Viscous permeability of random fiber structures: comparison of electrical and diffusional estimates with experimental and analytical results, J. Compos. Mater., 39 (2005) 163–188.
[30] B. Shapira, E. Avraham, D. Aurbach, Side reactions in capacitive deionization (CDI) processes: the role of oxygen reduction, Electrochim. Acta, 220 (2016) 285–295.
[31] M.S. Gaikwad, C. Balomajumder, Simultaneous electrosorptive removal of chromium(VI) and fluoride ions by capacitive deionization (CDI): multicomponent isotherm modeling and kinetic study, Sep. Purif. Technol., 186 (2017) 272–281.
[32] M.E. Suss, Size-based ion selectivity of micropore electric double layers in capacitive deionization electrodes, J. Electrochim. Soc., 9 (2017) 164.
[33] W.-W. Tang, D. He, C.-Y. Zhang, T.D. Waite, Optimization of sulfate removal from brackish water by membrane capacitive deionization (MCDI), Water Res., 121 (2017) 302–310.